International Journal of Automotive Technology, Vol. 6, No. 5, pp. 453–460 (2005)

1229-9138/2005/023-03

STUDY ON THE IN-CYLINDER FLOW CHARACTERISTICS OF AN SI ENGINE USING PIV

S.-Y. LEE[1], K.-S. JEONG[2], C.-H. JEON[1]* and Y.-J. CHANG[1]

[1]Department of Mechanical Engineering, RIMT, Pusan National University, Busan 609-735, Korea
[2]Department of Automotive Engineering, Jinju International University, Gyeongnam 660-845, Korea

(Received 16 March 2004; Revised 22 September 2004)

ABSTRACT–The tumble or swirl flow is used to promote mixing of air and fuel in the cylinder and to enlarge turbulent intensity in the end of the compression stroke. Since the in-cylinder flow is a kind of transient state with rapid flow variation, which is non-steady state flow, the tumble or swirl flow has not been analyzed sufficiently whether they are applicable to combustion theoretically. In the investigation of intake turbulent characteristics using PIV method, typical flow characteristics were figured out by SCV configurations. An engine installed SCV had higher vorticity and turbulent strength by fluctuation and turbulent kinetic energy than a baseline engine, especially near the cylinder wall and lower part of the cylinder. Above all, the engine with SCV B was superior to the others in aspect of vorticity and turbulent strength. For energy dissipation, a baseline engine had much higher energy loss than the engine installed SCV because flow impinged on the cylinder wall. Consequently, as swirl flow was added to existing tumble flow, it was found that fluctuation increased and flow energy was conserved effectively through the experiment.

KEY WORDS : PIV, Cross correlation, Swirl control valve, Flow visualization, Velocity vector

1. INTRODUCTION

An important factor in the configuration of the intake ports and the combustion chamber, in addition to the vaporization characteristics of the fuel, is the formation of flow fields within the vehicle engine. It has been reported that the flow field in the surrounding area of the flame during flame propagation in an SI engine is a determining factor in the combustion process, i.e. greatly affecting heat efficiency, engine performance, and emissions reduction (Hacohen *et al.*, 1994; Le, 1992). In this regard, a detailed analysis of the flow characteristics in the cylinder is necessary to devise a combustion acceleration method. Due to its mechanical configuration, the commonly used pentroof combustion chamber has an advantage in generating tumble flows as opposed to swirl flows. Many researchers have attempted to increase combustion efficiency by examining tumble flows: First, the spatial velocity distribution of the tumble flow field formation during initial intake is analyzed quantitatively. Second, the results are used in designing the intake ports and the combustion chamber. Finally, the turbulence generation process is analyzed (Ronnback *et al.*, 1991; Son *et al.*, 2004; Jeon *et al.*, 1998).

Current research concentrated upon turbulence flow field measurements, which were conducted using Hot Wire Anemometry (HWA) and Laser Doppler Velocimetry (LDV), to measure the average velocity and fluctuation. However, these are a point measurement methods, it is not appropriate for analyzing spatial flow field patterns. Currently used spatial measurement method is the Particle Image Velocimetry (PIV), which uses optical equipment, such as lasers, and computer-based digital imagery. The PIV system has not only many advantages of the LDV, but also can be used for comprehensively analyzing non-steady state flows, as well as quantitatively and qualitatively measuring spatial change (Lee *et al.*, 1993). Therefore, PIV is appropriate for flow measurements within the engine cylinder (Chang, 2004). The current research employs a steady-state flow experiment apparatus and PIV apparatus to measure the flow characteristics in a cylinder of a commercial pentroof gasoline engine. Specifically, the research focuses on the in-cylinder flow characteristics under several conditions: intake port configuration is changed, effect of the tumble flow, and results of different swirl control valve configurations. A 2-frame cross-correlation PIV technique was used to visualize the turbulence formation process within the combustion chamber during intake flow field intensification. Furthermore, speed, vorticity, flow intensity, turbulence intensity, energy loss, and other turbulence-specific factors were examined qualitatively

*Corresponding author. e-mail: chjeon@pusan.ac.kr

and quantitatively. These in turn were contrasted with the flow fields of baseline gasoline engines that were not affected by flow field intensification.

2. CROSS-CORRELATION PARTICLE IMAGE VELOCIMETRY TECHNIQUE

The velocity field of a certain flow can be measured by PIV. Unlike Particle Tracking Velocimetry (PTV), where one has to track each individual particle displacement, PIV employs an interrogation window.

The particle patterns in the interrogation window are analyzed. The particle displacement is tracked, and the displacement converted into velocity. The PIV technique used for the current research is a highly reliable technique called 2-frame cross-correlation PIV.

Figure 1 shows a schematic diagram for figuring out velocity vectors through cross-correlation processing.

An independent light source was used on each frame, and the flow fields were obtained by analyzing the particle displacement pattern from frame 1 to frame 2.

The displacement was calculated by an algorithm which employs 2-frame cross-correlation, and then it combined with the time difference of light pulses. By this analysis, velocity can be obtained.

In 2-frame cross-correlation, the first pulse is linked with the first frame and the second pulse is linked with the second frame. Due to both pulses are isolated and independent, ambiguity on the direction of the correlation peak is non-existent. Signal-to-Noise Ratio (SNR), which measured by 2-frame cross-correlation can be most accurately measured among all cross-correlation methods.

Figure 2 shows the distribution of cross-correlation coefficients. The cross-correlation function, $C(s)$, is combined with $C_C(s)$ and $C_F(s)$, which are dependent of the background and the correlation value of displacement components, and the maximum correlation value for both direction, $C_{D+}(s)$. The spatial correlation values of displacement have relatively large value because the particle displacements within a sequential pair of interrogation windows are nearly identical in direction over a short time frame. Finding these large values to determine the

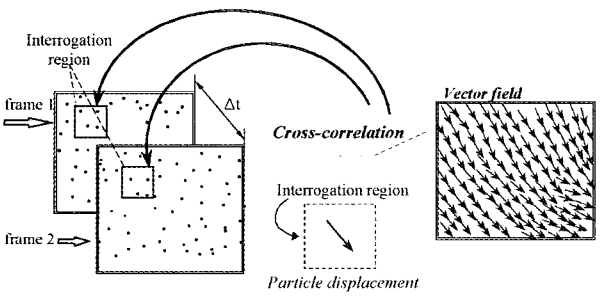

Figure 1. 2-frame cross-correlation processing.

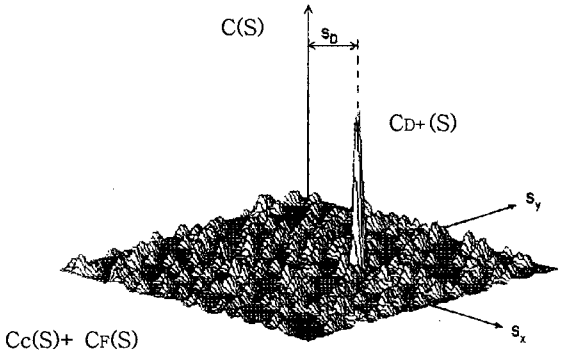

Figure 2. The distribution of cross-correlation coefficient and cross-correlation peak.

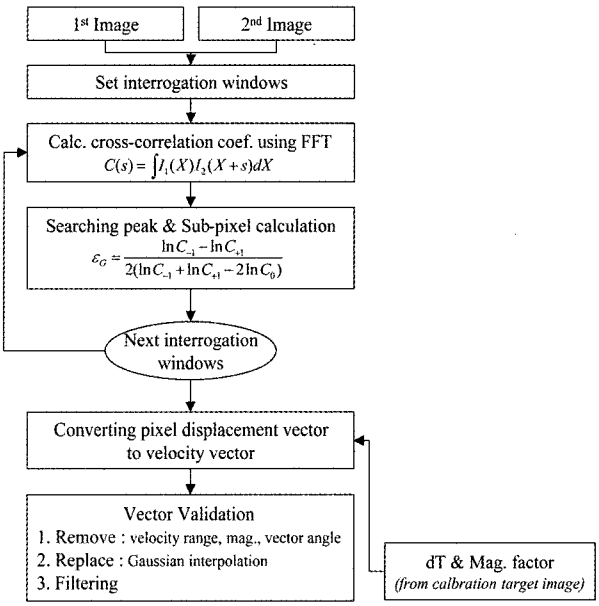

Figure 3. Block diagram of 2-frame cross-correlation method.

displacements is the basic idea behind cross-correlation particle displacement interrogation, and the basic equation is as follows:

$$C(s) = \int I_1(X)I_2(X+s)dX \quad (1)$$

$C(s)$ is the cross-correlation function, while I_1 and I_2 are the light intensities of the two sequential frames.

When I_1 and I_2 are obtained from different images, it is called a 2-frame cross-correlation method. The calculated cross-correlation distribution for the two frames is shown in Figure 2. In this figure, the coordinates of the maximum peak value represent the displacement of the particles in terms of pixel units. Figure 3 represents the block diagram for velocity field calculation processes via

2-frame cross-correlation.

3. EXPERIMENTAL APPARATUS AND PROCEDURE

3.1. Experimental Apparatus and Conditions

Figure 4 shows a schematic diagram of the PIV measurement system and gasoline engine steady-state flow experimental apparatus. The PIV system in the current research consists of a dual-pulse Nd:YAG laser system, which has energy intensity of 200 mJ and wavelength of 532 nm, a 1 K × 1 K high-resolution CCD camera (PIVCAM 10-15), synchronous apparatus (TSI 610032) to calculate velocity vector, and a data acquisition apparatus (insight NT 1.22). The insight NT 1.22 was only used to control the hardware system to obtain experiment data. A Nikon 50 mm standard-lens was attached to the CCD camera to minimize image distortion errors. The time interval between 2-frames was used to set optimum value according to the velocity of flow field. When the time interval sets longer than 35 μs, this results make it possible to measure low-speed images only. The reason is that the high-speed images were out of measurement boundary. On the contrary, when the time interval sets shorter than 35 μs, it only measured high-speed images in accordance with small images displacement. Therefore, as the result of research work, optimal time interval between 2 frames is determined 35 μs that is considered the best cross-correlation as images displacement. It could be taken the measurement of turbulent flows in cylinder. The laser beam was projected through a cylindrical lens to create a laser sheet to use in the flow analysis, and the CCD camera was set up perpendicularly to the laser sheet to obtain the particle images.

The steady-state flow experimental apparatus consists of a blower for air inflow. The blower specifications are maximum pressure of 1.2 atm, output of 7.5 kW, and flow of 5.6 m^3/min. To measure intake flow, a laminar flowmeter was installed, and pressure differences were measured in the 1–1000 mmH_2O range with a micro-manometer. Furthermore, the experiment was conducted the pressure difference between the multi intake port and in-cylinder at a constant 250 mmH_2O. The cylinder head used in the research was a pentroof 2000cc, SOHC, with an acrylic tumble adapter attached to the first cylinder to facilitate the measurements. The tumble adapter was 5 mm thick and had an inner diameter identical to the cylinder diameter of 85 mm. Laskin nozzles, which apply the principle of cavitations, were used to produce olive oil aerosol.

Table 1. Experimental condition.

Visual field	Cylinder center			
SCV types	Baseline	SCV A	SCV B	SCV C
Open ratio (%)	100	89	72.5	78
Valve lift (mm)	2, 4, 6, 8			
Interval of 2 frames	$\Delta t \geq 35$ μs			
Intake differential pressure	250mmH_2O			

The aerosol was used as tracking particles in this research, and it was appropriate to use in PIV of fluid flows with an average diameter of 2 μm (Melling, 1997). Table 1 shows the experimental conditions for the SCV and intake valve lifts that were used for examining flow aspects. Figure 5 is the SCV configurations, which show position and open ratio of the SCV. The selected SCV minimizes the flux coefficient loss while maximizing the swirl intensity throughout trial and error experiments about eighty times. Furthermore, the intake valve lift was increased at 2 mm intervals over 2 mm–8 mm, and the flow field was measured to find and compare the turbulence characteristics.

3.2. Velocity Vector Calculation and Post-processing

The algorithm used to obtain velocity vectors was the 2-

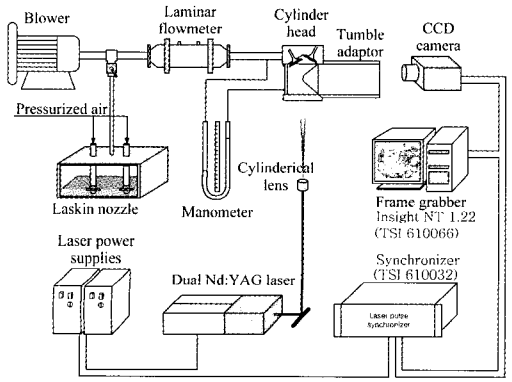

Figure 4. Schematic diagram of experimental apparatus.

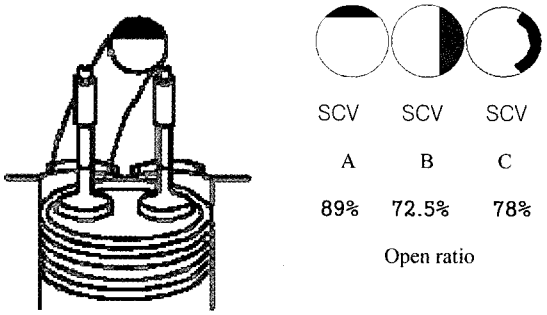

Figure 5. Configurations of SCV.

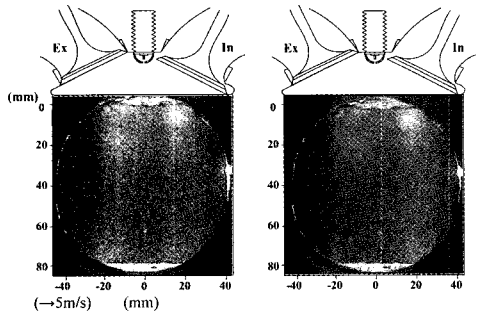

(a) Frame 1 (b) Frame 2

Figure 6. Instantaneous raw images in cylinder (Δt = 35 μs).

frame cross-correlation technique. For the velocity vector, there are 6400(80 × 80) lattice numbers and the spatial resolution between vectors is 0.93 mm. The actual length of one pixel is 0.096 mm, and software inaccuracies occur during subpixel tracking, which is a result of image resolution limitations. The interrogation region for finding the maximum cross-correlation coefficient is 24 × 24 pixels in size. The actual size of the interrogation region is approximately 2.304 mm with a 50% overlap allowance.

The velocity vectors obtained through the above technique were processed through the PIV ACE 1.0 processing program for post-processing such as eliminating fault validation vectors, centroid track, ensemble averaging and interpolation, as well as for obtaining statistical measures. By comparing the absolute values of the u, v vector, the pre-process velocity vectors were validated, and eliminate the error vectors considering the magnitude and direction of surrounding vectors. This was followed by a process where the vector values are converted from pixel units to actual velocity vector units (m/s) and the velocity vector were extracted.

The 510 instances of velocity fields were obtained from 1020 images for each case, and these were ensemble averaged to obtain the average flow field.

4. RESULTS AND ANALYSIS

4.1. Fluid Drift Distribution within the Engine Cylinder

Figure 6 shows the raw images of the in-cylinder instantaneous flow field which viewed along the central axis of a gasoline engine. The time interval between the first and second frames is 35 μs. The tiny and white particles in the raw images are the olive oil tracking particles scatted light from the laser sheet.

Figure 7 shows the instantaneous velocity fields obtained the digitally processed raw images by using cross-correlation PIV. 1020 raw images were taken and 510 velocity fields were obtained. This figure represents the instantaneous velocity field of the baseline engine,

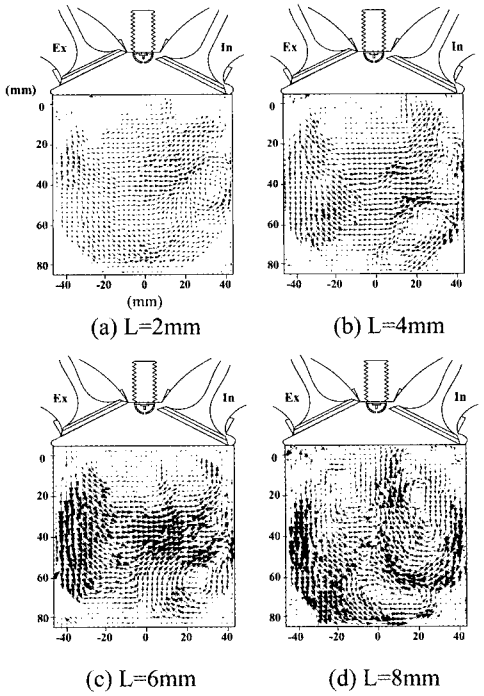

(a) L=2mm (b) L=4mm

(c) L=6mm (d) L=8mm

Figure 7. Instantaneous velocity field of baseline engine.

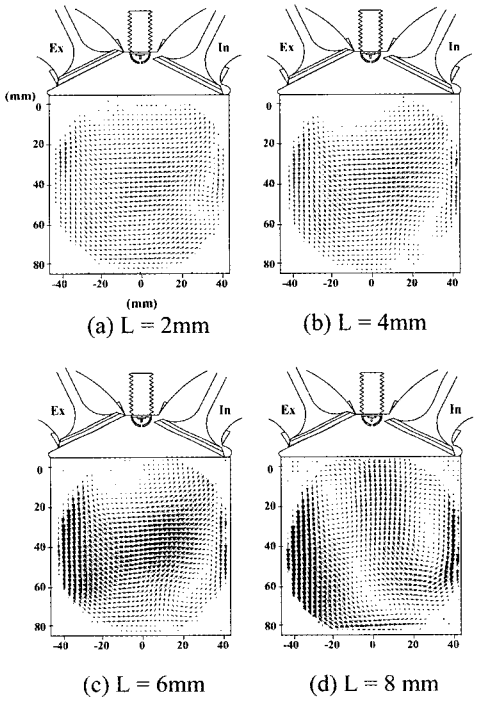

(a) L = 2mm (b) L = 4mm

(c) L = 6mm (d) L = 8 mm

Figure 8. The ensemble averaged velocity field of baseline engine.

which did not attach the swirl controller valve, as varying 2 mm valve lift in the range of 2–8 mm. The results by

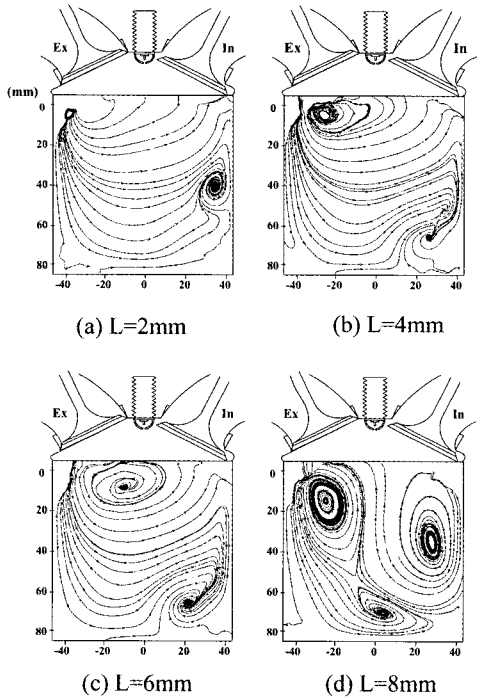

Figure 9. The streamline from ensemble averaged velocity field (baseline engine).

using ACE 1.0 processing program are presented in Figures 8 and 9.

Figure 8 shows the flow field taken by the ensemble averaged of the 510 instantaneous velocity field and Figure 9 show the flow field where the velocity vectors have been streamlined in order to more closely examine the direction of the velocity vectors.

It can be observed that, under low valve lift conditions, the tumble flow, the counter-clockwise rotational flow, beneath the exhaust port is larger than the clockwise rotational backward tumble flow beneath the intake port. The tumble flows are the result of intake flows turning into rotational flow due to the design of the valves and the combustion chamber. The intake flow turns into the rational flow whether the intake flow hits into or follows the contours of the cylinder walls. Also, it can clearly be observed that a vortex is created in the lower part of intake valve, central part of the cylinder as the clockwise rotational flow backward tumble comes down the right-hand cylinder wall. As the valve lift is increased, the backward tumble is also intensified, and three vortices are created at maximum lift.

4.2. In-cylinder Flow Characteristics with Addition of Swirl Control Valve

Figure 10 shows the velocity vectors of in-cylinder tumble formation and flow characteristics in the stage of

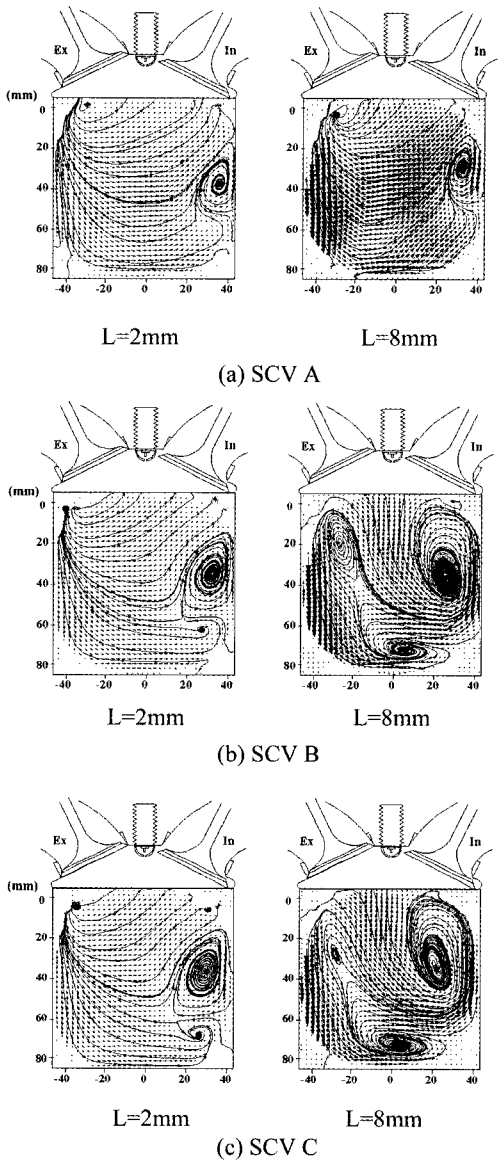

Figure 10. Ensemble averaged velocity field and streamline (SCV-attached engine).

intake stroke. The SCV is attached to the intake port and it adds a swirl component to the tumble flow. The SCV configuration was identical to that of Figure 5, which was in turn selected via steady-state flow experiments.

Figure 10 shows the structure of flow fields when the valve lift was at 2 mm and 8 mm. The six flow visualizations were shown in Figure 10. These flow fields depend on valve lift and SCV configuration. In the case of Figure 10(a), an intensity counter-clockwise tumble flow as the maximum velocity of 7.2 m/s throughout valve lift prevents the formation of the vortex that was observed in the lower, central part of the baseline engine cylinder. It can also be observed that the flow is guided

towards the upper, right-hand side of the cylinder. Furthermore, it can be observed that a backward tumble flow as the maximum velocity of 5.1 m/s is formed on the right-hand cylinder wall, but it is small compared to the other patterns. In Figure 10(b), (c), it can be seen that B and C valve makes not only the tumble flow but also the backward tumble flow. Due to a collision between the tumble flow and the backward tumble flow on cylinder wall sides and a friction between the rotating swirl flow and the tumble flow, the direction of the flow changed and then the inclined tumble may be seen.

4.3. In-cylinder Distribution of Vorticity

In general, an increase of vorticity results in an effect of mixing with oxidizing agent, and increase of the combustion acceleration effect. Vorticity is usually represented as the rotating of the velocity vector, and is defined as follows:

$$\omega = \frac{1}{2}\left(\frac{\partial v}{\partial x} - \frac{\partial u}{\partial y}\right) \tag{2}$$

The signs of the vorticity represent the direction of the rotation. Figure 11 shows the in-cylinder vorticity distribution at maximum valve lift of 8 mm. These figures show the average flow fields of 510 instantaneous velocity fields. From the figures, it can be seen that there is a tendency that the vorticity near the both sides of the cylinder wall has a greater value than the central part of the cylinder. Overall, vorticity effects were greater in the engines attached SCV than the baseline engine. Particularly SCV B has greater vorticity than the others.

4.4. In-cylinder Distribution of Turbulence Intensity

Instantaneous velocity, u_i, is a meaningful physical value of turbulence velocity, and can be broken down into mean velocity, U_i, and fluctuation velocity, u'_i.

$$u_i = U_i + u_i' \quad v = V_i + v_i' \tag{3}$$

The fluctuation intensities of turbulence are represented by $\sqrt{u'^2}$ $\sqrt{v'^2}$ and can be used to represent turbulence intensity as follows.

$$u_{rms} = \sqrt{\overline{u'^2}} \quad v_{rms} = \sqrt{\overline{v'^2}} \tag{4}$$

The value of u_{rms} represents the horizontal fluctuation velocity, and has strongest value at the point where the flows collide and create vortices. Fluctuation effects were more widely distributed for swirl flow intensified engines as compared to the baseline engines. The value of v_{rms} represents the vertical turbulence fluctuation velocity, and has strongest value near the cylinder walls.

The SCV B and C, which has greater swirl flows, affects vertical turbulence fluctuation velocities, as well as horizontal. Figures 12 and 13 compare the turbulence intensity according to engine valve lift for the engine attached SCV and the baseline engines. These results were obtained by integrating the turbulence intensity over

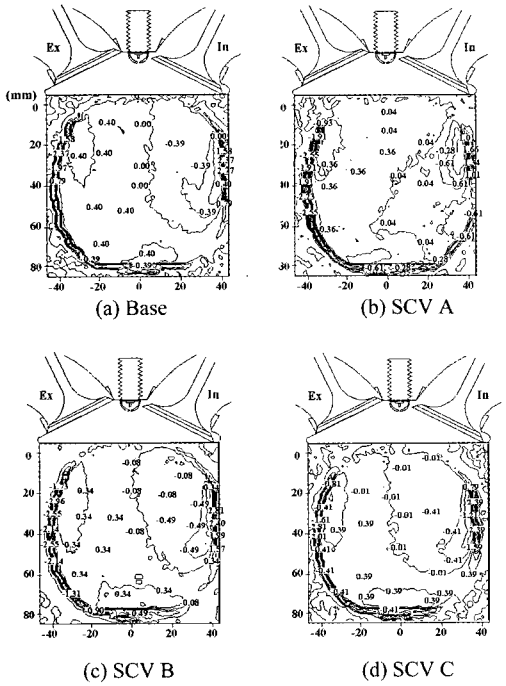

Figure 11. Vorticity distribution in cylinder (L = 8 mm).

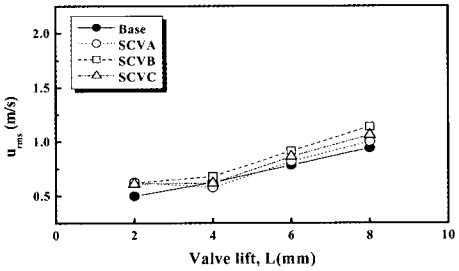

Figure 12. Comparison of fluctuation component (U_{rms}) according to valve lift.

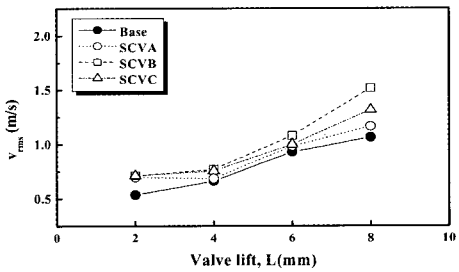

Figure 13. Comparison of fluctuation component (v_{rms}) according to valve lift.

the entire visualized region. As discussed previously, turbulence was more intense for engines with SCV C, and A. It can be determined turbulence is intensified when swirl flows are added to the existing tumble flows. Further, it can be seen that the degree of in-cylinder turbulence fluctuation is affected 1.39 times more by the vertical fluctuation component as opposed to the horizontal one. It can be assumed from this result that the kinetic energy transfer quantity due to vertical turbulence fluctuation is more active.

4.5. In-cylinder Distribution of Energy Dissipation

Figure 14 shows the in-cylinder dissipation energy distribution for the baseline and the engines attached SCV at valve lift of 8 mm. In order to find the energy distribution of the flow, it allows the grasping of energy destroy and find energy conservation. Energy dissipation, D, was defined as follow, where the dissipation is the integral of the entire in-cylinder flow field.

$$D = \mu\left[2\left(\frac{\partial u}{\partial x}\right)^2 + \left(\frac{\partial v}{\partial y}\right)^2 + \left(\frac{\partial v}{\partial x} + \frac{\partial u}{\partial y}\right)^2\right] \quad (5)$$

In the above equation μ is the viscosity coefficient of the fluid. Energy dissipation is greater as 9.052×10^{-4} W/kg in the baseline engine than in the SCV A, B and C engines as 4.1567, 2.896 and 2.785×10^{-4} W/kg for 8 mm valve lift respectively, and there is considerable energy destroy as the flow crashes into the cylinder walls. The energy dissipation rate is low for the lower zone of the

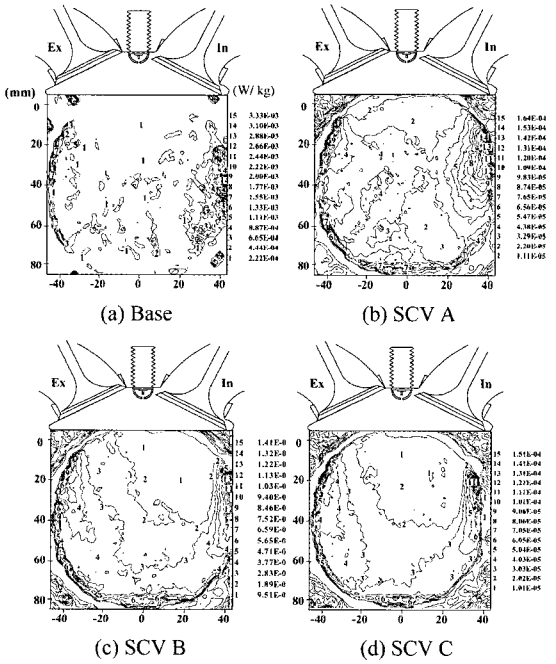

Figure 14. Dissipation energy distribution in cylinder (L = 8 mm).

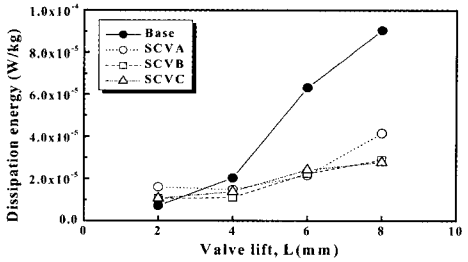

Figure 15. Comparison of dissipation energy according to valve lift.

baseline engine, however, for the SCV- fitted engines.

There is a great deal of energy destroys due to the collision of 1) the backward tumble that flows downward from the right-hand cylinder wall, and 2) the downward flow from the left-hand cylinder wall. These effects are minimized as the flows rise towards the top of the cylinder and become stable. Figure 15 shows the comparison of dissipation energy according to valve lift. Energy dissipation increases greatly with increase of the valve lift for the baseline engine. Among the SCV configurations, valves B and C show the least dissipation which means these configurations are best for energy conservation.

5. CONCLUSIONS

This paper studied the flow aspects of the in-cylinder turbulent flow fields of a pentroof gasoline engine. The tumble flow which is formed at the port during intake and changed the flow conditions by SCV, were analyzed using a steady-state flow experimental apparatus and 2-frame cross-correlation PIV technique. The following conclusions were obtained from quantitative and qualitative analysis of the turbulence characteristics with changes of the valve lift and SCV configurations.

(1) From the flow field of the baseline engine as varying valve lifts between 2 mm and 8 mm, it was visually confirmed that at low lifts tumble flows were dominant over backward tumble. The Increase of the valve lift results not only the increases of tumble flow but also the increases of backward tumble flow. At the maximum valve lift, the wall frictions and flow collisions led to the formation of three large vortices.

(2) With an addition of SCV, the flow characteristics changed by the open ratio and configuration of the SCV. For valve configuration A, the tumble flow was strong as the maximum velocity of 7.2 m/s. Valve configurations B and C had similarly strong tumble flows, in addition to strong backward tumble as the maximum velocity of 5.1 m/s; the collision between

these two flows. The swirl flow affects the central direction of the entire flow and makes the inclined tumbles.

(3) In-cylinder distribution of flow field vorticity was greater in the engines attached SCV comparing to the baseline engines. Vorticity was strongest near the cylinder walls, and decreased towards the center of the cylinder. Vorticity was strongest for SCV B, followed by SCV C, then SCV A. This was the result of adding a swirl component to the original tumble flow.

(4) Turbulence intensity due to fluctuation has strongest value at the point where vortices were formed from flow collisions. The effects from fluctuation were more widely distributed for the swirl-flow-intensified engines as opposed to the baseline engine. Furthermore, the turbulence fluctuation in the vertical direction was 1.39 times than in the horizontal direction with increase of the valve lift.

(5) Energy dissipation was greater as 9.052×10^{-4} W/kg in the baseline engine than in the engines attached SCV A, B and C as 4.1567, 2.896 and 2.785×10^{-4} W/kg for 8mm valve lift respectively. A large degree of energy destroy occurs as the flow collided against the cylinder walls. In the lower part of the cylinder, the dissipation rate was low for the baseline engine. Due to flow collisions, the dissipation rate of the SCV engine is great. Based on the results of all the SCV configurations, SCV B and SCV C have the lowest energy dissipation for all valve lifts. It is no doubt that these two configurations are the best for energy conservation.

REFERENCES

Chang, T. H. (2004). Experimental study on turbulent swirling flow in a cylindrical annuli by using the PIV technique. *Int. J. Automotive Technology* **5**, **1**, 17–22.

Chang, T. H. (2004). Experimental study on turbulent swirling flow in a cylindrical annuli by using the PIV technique. *Int. J. Automotive Technology* **5**, **1**, 17–22.

Cho, G. B., Jeon, C. H., Chang, Y. J. and Kang, K. Y. (1997). Characteristics of in-cylinder steady flow using PIV for different intake port geometries in a 4-valve gasoline engine. *Trans. Korean Society Automotive Engineers* **5**, **5**, 188–196.

Hacohen, J., Beltmont, M. R. and Ashcroft, S. J. (1994). Flame speeds in a spark ignition engine. *SAE Paper No.* 942050.

Jeon, C. H., Chang, Y. J. Cho, K. B. and Kang, K. Y. (1998). Effects of intake ports on in-cylinder flow and lean combustion in a 4-valve engine. *SAE Paper No.* 981048.

Lee, J. H. and Farrell, P. V. (1993). Intake valve measurement of an in engine using particle image velocimetry. *SAE Paper No.* 930480.

Lee, K. H., Lee, C. S., Lee, H, G., Chon, M. S. and Joo, Y. C. (1998). Spatial analysis of turbulent flow in combustion chamber using high resolution dual color PIV. *Trans. KSME* **6**, **6**, 132–141.

Le Coz, J. F. (1992). Cycle-to-cycle correlations between flow field and combustion initiation in a SI Engine. *SAE Paper No.* 920517.

Melling, A. (1997). Tracer particles and seeding for particle image velocimetry. *Meas. Sci. Technology* **8**, 1406–1416.

Park, J. H., Lee, N. H. and Choi, K. H. (1999). Analysis of in-cylinder flow fields using particle image velocimetry. *Trans. Korean Society Automotive Engineers* **7**, **4**, 46–53.

Ronnback, M., Le, W. X. and Linna, J. R. (1991). Study of induction tumble by particle tracking velocimetry in a 4-valve engine. *SAE Paper No.* 912376.

Son, J. W., Lee, S. H., Han, B. H. and Kim, W. T. (2004). A correlation between re-defined design parameters and flow coefficients of SI engine intake ports. *SAE Paper No.* 2004-01-0998.